Up and Down Quark Structure of the Proton

V.M. Abazov,[31] B. Abbott,[66] B.S. Acharya,[25] M. Adams,[45] T. Adams,[43] J.P. Agnew,[40] G.D. Alexeev,[31] G. Alkhazov,[35] A. Alton[a],[55] A. Askew,[43] S. Atkins,[53] K. Augsten,[7] C. Avila,[5] F. Badaud,[10] L. Bagby,[44] B. Baldin,[44] D.V. Bandurin,[73] S. Banerjee,[25] E. Barberis,[54] P. Baringer,[52] J.F. Bartlett,[44] U. Bassler,[15] V. Bazterra,[45] A. Bean,[52] M. Begalli,[2] L. Bellantoni,[44] S.B. Beri,[23] G. Bernardi,[14] R. Bernhard,[19] I. Bertram,[38] M. Besançon,[15] R. Beuselinck,[39] P.C. Bhat,[44] S. Bhatia,[57] V. Bhatnagar,[23] G. Blazey,[46] S. Blessing,[43] K. Bloom,[58] A. Boehnlein,[44] D. Boline,[63] E.E. Boos,[33] G. Borissov,[38] A. Brandt,[70] O. Brandt,[20] M. Brochmann,[74] R. Brock,[56] A. Bross,[44] D. Brown,[14] X.B. Bu,[44] M. Buehler,[44] V. Buescher,[21] V. Bunichev,[33] S. Burdin[b],[38] C.P. Buszello,[37] E. Camacho-Pérez,[28] B.C.K. Casey,[44] H. Castilla-Valdez,[28] S. Caughron,[56] S. Chakrabarti,[63] K.M. Chan,[50] A. Chandra,[72] E. Chapon,[15] G. Chen,[52] S.W. Cho,[27] S. Choi,[27] B. Choudhary,[24] S. Cihangir[‡],[44] D. Claes,[58] J. Clutter,[52] M. Cooke[j],[44] W.E. Cooper,[44] M. Corcoran[‡],[72] F. Couderc,[15] M.-C. Cousinou,[12] J. Cuth,[21] D. Cutts,[69] A. Das,[71] G. Davies,[39] S.J. de Jong,[29, 30] E. De La Cruz-Burelo,[28] F. Déliot,[15] R. Demina,[62] D. Denisov,[64] S.P. Denisov,[34] S. Desai,[44] C. Deterre[c],[40] K. DeVaughan,[58] H.T. Diehl,[44] M. Diesburg,[44] P.F. Ding,[40] A. Dominguez,[58] A. Drutskoy[q],[32] A. Dubey,[24] L.V. Dudko,[33] A. Duperrin,[12] S. Dutt,[23] M. Eads,[46] D. Edmunds,[56] J. Ellison,[42] V.D. Elvira,[44] Y. Enari,[14] H. Evans,[48] A. Evdokimov,[45] V.N. Evdokimov,[34] A. Fauré,[15] L. Feng,[46] T. Ferbel[‡],[62] F. Fiedler,[21] F. Filthaut,[29, 30] W. Fisher,[56] H.E. Fisk[‡],[44] M. Fortner,[46] H. Fox,[38] J. Franc,[7] S. Fuess,[44] P.H. Garbincius,[44] A. Garcia-Bellido,[62] J.A. García-González,[28] V. Gavrilov,[32] W. Geng,[12, 56] C.E. Gerber,[45] Y. Gershtein,[59] G. Ginther,[44] G. Golovanov[‡],[31] P.D. Grannis,[63] S. Greder,[16] H. Greenlee,[44] G. Grenier,[17] Ph. Gris,[10] J.-F. Grivaz,[13] A. Grohsjean[c],[15] S. Grünendahl,[44] M.W. Grünewald,[26] T. Guillemin,[13] G. Gutierrez,[44] P. Gutierrez,[66] J. Haley,[67] L. Han,[4] K. Harder,[40] A. Harel,[62] J.M. Hauptman,[51] J. Hays,[39] T. Head,[40] T. Hebbeker,[18] D. Hedin,[46] H. Hegab,[67] A.P. Heinson,[42] U. Heintz,[69] C. Hensel,[1] I. Heredia-De La Cruz[d],[28] K. Herner,[44] G. Hesketh[f],[40] M.D. Hildreth,[50] R. Hirosky,[73] T. Hoang,[43] J.D. Hobbs,[63] B. Hoeneisen,[9] J. Hogan,[72] M. Hohlfeld,[21] J.L. Holzbauer,[57] I. Howley,[70] Z. Hubacek,[7, 15] V. Hynek,[7] I. Iashvili,[61] Y. Ilchenko,[71] R. Illingworth,[44] A.S. Ito,[44] S. Jabeen[m],[44] M. Jaffré,[13] A. Jayasinghe,[66] M.S. Jeong,[27] R. Jesik,[39] P. Jiang[‡],[4] K. Johns,[41] E. Johnson,[56] M. Johnson,[44] A. Jonckheere,[44] P. Jonsson,[39] J. Joshi,[42] A.W. Jung[o],[44] A. Juste,[36] E. Kajfasz,[12] D. Karmanov,[33] I. Katsanos,[58] M. Kaur,[23] R. Kehoe,[71] S. Kermiche,[12] N. Khalatyan,[44] A. Khanov,[67] A. Kharchilava,[61] Y.N. Kharzheev,[31] I. Kiselevich,[32] J.M. Kohli,[23] A.V. Kozelov[‡],[34] J. Kraus,[57] A. Kumar,[61] A. Kupco,[8] T. Kurča,[17] V.A. Kuzmin,[33] S. Lammers,[48] P. Lebrun,[17] H.S. Lee,[27] S.W. Lee,[51] W.M. Lee[‡],[44] X. Lei,[41] J. Lellouch,[14] D. Li,[14] H. Li,[73] L. Li,[42] Q.Z. Li,[44] J.K. Lim,[27] D. Lincoln,[44] J. Linnemann,[56] V.V. Lipaev[‡],[34] R. Lipton,[44] H. Liu,[71] Y. Liu,[4] A. Lobodenko,[35] M. Lokajicek[‡],[8] R. Lopes de Sa,[44] R. Luna-Garcia[g],[28] A.L. Lyon,[44] A.K.A. Maciel,[1] R. Madar,[19] R. Magaña-Villalba,[28] S. Malik,[58] V.L. Malyshev,[31] J. Mansour,[20] J. Martínez-Ortega,[28] R. McCarthy,[63] C.L. McGivern,[40] M.M. Meijer,[29, 30] A. Melnitchouk,[44] D. Menezes,[46] P.G. Mercadante,[3] M. Merkin,[33] A. Meyer,[18] J. Meyer[i],[20] F. Miconi,[16] N.K. Mondal,[25] M. Mulhearn,[73] E. Nagy,[12] M. Narain[‡],[69] R. Nayyar,[41] H.A. Neal[‡],[55] J.P. Negret,[5] P. Neustroev,[35] H.T. Nguyen,[73] T. Nunnemann,[22] J. Orduna,[69] N. Osman,[12] A. Pal,[70] N. Parashar,[49] V. Parihar,[69] S.K. Park,[27] R. Partridge[e],[69] N. Parua,[48] A. Patwa[j],[64] B. Penning,[39] M. Perfilov,[33] Y. Peters,[40] K. Petridis,[40] G. Petrillo,[62] P. Pétroff,[13] M.-A. Pleier,[64] V.M. Podstavkov,[44] A.V. Popov,[34] M. Prewitt,[72] D. Price,[40] N. Prokopenko,[34] J. Qian,[55] A. Quadt,[20] B. Quinn,[57] P.N. Ratoff,[38] I. Razumov,[60] I. Ripp-Baudot,[16] F. Rizatdinova,[67] M. Rominsky,[44] A. Ross,[38] C. Royon,[52] P. Rubinov,[44] R. Ruchti,[50] G. Sajot,[11] A. Sánchez-Hernández,[28] M.P. Sanders,[22] A.S. Santos[h],[1] G. Savage,[44] L. Sawyer,[53] T. Scanlon,[39] R.D. Schamberger,[63] Y. Scheglov[‡],[35] H. Schellman,[68, 47] M. Schott,[21] C. Schwanenberger[c],[40] R. Schwienhorst,[56] J. Sekaric,[52] H. Severini,[66] E. Shabalina,[20] V. Shary,[15] S. Shaw,[40] A.A. Shchukin,[34] V. Simak[‡],[7] P. Skubic,[66] P. Slattery,[62] G.R. Snow[‡],[58] J. Snow,[65] S. Snyder,[64] S. Söldner-Rembold,[40] L. Sonnenschein,[18] K. Soustruznik,[6] J. Stark,[11] D.A. Stoyanova,[34] M. Strauss,[66] L. Suter,[40] P. Svoisky,[73] M. Titov,[15] V.V. Tokmenin,[31] Y.-T. Tsai,[62] D. Tsybychev,[63] B. Tuchming,[15] C. Tully,[60] L. Uvarov,[35] S. Uvarov,[35] S. Uzunyan,[46] R. Van Kooten,[48] W.M. van Leeuwen,[29] N. Varelas,[45] E.W. Varnes,[41] I.A. Vasilyev,[34] A.Y. Verkheev,[31] L.S. Vertogradov,[31] M. Verzocchi,[44] M. Vesterinen,[40] D. Vilanova,[15] P. Vokac,[7] H.D. Wahl,[43] C. Wang,[4] M.H.L.S. Wang,[44] J. Warchol[‡],[50] G. Watts,[74] M. Wayne,[50] J. Weichert,[21] L. Welty-Rieger,[47] M.R.J. Williams[n],[48] G.W. Wilson,[52] M. Wobisch,[53] D.R. Wood,[54] T.R. Wyatt,[40] M. Xie,[4] Y. Xie,[44] R. Yamada[‡],[44]

S. Yang,[4] T. Yasuda,[44] Y.A. Yatsunenko[‡],[31] W. Ye,[63] Z. Ye,[44] H. Yin,[44] K. Yip,[64] S.W. Youn,[44] J.M. Yu,[55] J. Zennamo,[61] T.G. Zhao,[40] B. Zhou,[55] J. Zhu,[55] M. Zielinski,[62] D. Zieminska,[48] and L. Zivkovic[p][14]

(The D0 Collaboration[*])

[1]LAFEX, Centro Brasileiro de Pesquisas Físicas, Rio de Janeiro, RJ 22290, Brazil
[2]Universidade do Estado do Rio de Janeiro, Rio de Janeiro, RJ 20550, Brazil
[3]Universidade Federal do ABC, Santo André, SP 09210, Brazil
[4]University of Science and Technology of China, Hefei 230026, People's Republic of China
[5]Universidad de los Andes, Bogotá, 111711, Colombia
[6]Charles University, Faculty of Mathematics and Physics,
Center for Particle Physics, 116 36 Prague 1, Czech Republic
[7]Czech Technical University in Prague, 116 36 Prague 6, Czech Republic
[8]Institute of Physics, Academy of Sciences of the Czech Republic, 182 21 Prague, Czech Republic
[9]Universidad San Francisco de Quito, Quito 170157, Ecuador
[10]LPC, Université Blaise Pascal, CNRS/IN2P3, Clermont, F-63178 Aubière Cedex, France
[11]LPSC, Université Joseph Fourier Grenoble 1, CNRS/IN2P3,
Institut National Polytechnique de Grenoble, F-38026 Grenoble Cedex, France
[12]CPPM, Aix-Marseille Université, CNRS/IN2P3, F-13288 Marseille Cedex 09, France
[13]LAL, Univ. Paris-Sud, CNRS/IN2P3, Université Paris-Saclay, F-91898 Orsay Cedex, France
[14]LPNHE, Universités Paris VI and VII, CNRS/IN2P3, F-75005 Paris, France
[15]IRFU, CEA, Université Paris-Saclay, F-91191 Gif-Sur-Yvette, France
[16]IPHC, Université de Strasbourg, CNRS/IN2P3, F-67037 Strasbourg, France
[17]IPNL, Université Lyon 1, CNRS/IN2P3, F-69622 Villeurbanne Cedex,
France and Université de Lyon, F-69361 Lyon CEDEX 07, France
[18]III. Physikalisches Institut A, RWTH Aachen University, 52056 Aachen, Germany
[19]Physikalisches Institut, Universität Freiburg, 79085 Freiburg, Germany
[20]II. Physikalisches Institut, Georg-August-Universität Göttingen, 37073 Göttingen, Germany
[21]Institut für Physik, Universität Mainz, 55099 Mainz, Germany
[22]Ludwig-Maximilians-Universität München, 80539 München, Germany
[23]Panjab University, Chandigarh 160014, India
[24]Delhi University, Delhi-110 007, India
[25]Tata Institute of Fundamental Research, Mumbai-400 005, India
[26]University College Dublin, Dublin 4, Ireland
[27]Korea Detector Laboratory, Korea University, Seoul, 02841, Korea
[28]CINVESTAV, Mexico City 07360, Mexico
[29]Nikhef, Science Park, 1098 XG Amsterdam, the Netherlands
[30]Radboud University Nijmegen, 6525 AJ Nijmegen, the Netherlands
[31]Joint Institute for Nuclear Research, Dubna 141980, Russia
[32]Institute for Theoretical and Experimental Physics, Moscow 117259, Russia
[33]Moscow State University, Moscow 119991, Russia
[34]Institute for High Energy Physics, Protvino, Moscow region 142281, Russia
[35]Petersburg Nuclear Physics Institute, St. Petersburg 188300, Russia
[36]Institució Catalana de Recerca i Estudis Avançats (ICREA) and Institut
de Física d'Altes Energies (IFAE), 08193 Bellaterra (Barcelona), Spain
[37]Uppsala University, 751 05 Uppsala, Sweden
[38]Lancaster University, Lancaster LA1 4YB, United Kingdom
[39]Imperial College London, London SW7 2AZ, United Kingdom
[40]The University of Manchester, Manchester M13 9PL, United Kingdom
[41]University of Arizona, Tucson, Arizona 85721, USA
[42]University of California Riverside, Riverside, California 92521, USA
[43]Florida State University, Tallahassee, Florida 32306, USA
[44]Fermi National Accelerator Laboratory, Batavia, Illinois 60510, USA
[45]University of Illinois at Chicago, Chicago, Illinois 60607, USA
[46]Northern Illinois University, DeKalb, Illinois 60115, USA
[47]Northwestern University, Evanston, Illinois 60208, USA
[48]Indiana University, Bloomington, Indiana 47405, USA
[49]Purdue University Calumet, Hammond, Indiana 46323, USA
[50]University of Notre Dame, Notre Dame, Indiana 46556, USA
[51]Iowa State University, Ames, Iowa 50011, USA
[52]University of Kansas, Lawrence, Kansas 66045, USA
[53]Louisiana Tech University, Ruston, Louisiana 71272, USA
[54]Northeastern University, Boston, Massachusetts 02115, USA
[55]University of Michigan, Ann Arbor, Michigan 48109, USA
[56]Michigan State University, East Lansing, Michigan 48824, USA

[57]University of Mississippi, University, Mississippi 38677, USA
[58]University of Nebraska, Lincoln, Nebraska 68588, USA
[59]Rutgers University, Piscataway, New Jersey 08855, USA
[60]Princeton University, Princeton, New Jersey 08544, USA
[61]State University of New York, Buffalo, New York 14260, USA
[62]University of Rochester, Rochester, New York 14627, USA
[63]State University of New York, Stony Brook, New York 11794, USA
[64]Brookhaven National Laboratory, Upton, New York 11973, USA
[65]Langston University, Langston, Oklahoma 73050, USA
[66]University of Oklahoma, Norman, Oklahoma 73019, USA
[67]Oklahoma State University, Stillwater, Oklahoma 74078, USA
[68]Oregon State University, Corvallis, Oregon 97331, USA
[69]Brown University, Providence, Rhode Island 02912, USA
[70]University of Texas, Arlington, Texas 76019, USA
[71]Southern Methodist University, Dallas, Texas 75275, USA
[72]Rice University, Houston, Texas 77005, USA
[73]University of Virginia, Charlottesville, Virginia 22904, USA
[74]University of Washington, Seattle, Washington 98195, USA

We measure proton structure parameters sensitive primarily to valence quarks using 8.6 fb^{-1} of data collected by the D0 detector in $\sqrt{s} = 1.96$ TeV $p\bar{p}$ collisions at the Fermilab Tevatron. We exploit the property of the forward-backward asymmetry in dilepton events to be factorized into distinct structure parameters and electroweak quark-level asymmetries. Contributions to the asymmetry from s, c and b quarks, as well as from u and d sea quarks, are suppressed allowing valence u and d quarks to be separately determined. We find an u to d quark ratio near the peak values in the quark density distributions that is smaller than predictions from modern parton distribution functions.

The forward-backward asymmetry, A_{FB}, in dilepton production at hadron colliders is due to parity violation in the electroweak interaction but also depends upon the hadron's partonic structure [1–4]. Although many observables depend upon the experimentally indistinguishable contributions from different quark flavors, A_{FB} has the capability to provide information on specific quarks. Contributions to A_{FB} from the s, c and b quarks are significantly suppressed because the quark and antiquark densities are nearly the same and thus A_{FB} predominately depends on u and d quark densities. Moreover, the asymmetries for $u\bar{u}$ and $d\bar{d}$ initial states depend differently on the dilepton mass (M), offering the possibility to obtain u and d quark densities individually. Recent analyses [5, 6] show that A_{FB} can be factorized into sep-

arate electroweak and quantum chromodynamics (QCD) functions allowing independent determinations of the effective weak mixing angle parameter $\sin^2 \theta_{\rm eff}^{\ell}$, and proton structure parameters called P_u and P_d for u and d quarks, respectively. Measurements of P_u and P_d provide unique information about the proton structure.

In this paper we report a determination of P_u and P_d from the A_{FB} distributions in $p\bar{p} \to Z/\gamma^* \to \ell^+\ell^-$ events using data corresponding to 8.6 fb^{-1} of integrated luminosity collected with the D0 detector at the Fermilab Tevatron $p\bar{p}$ collider at $\sqrt{s} = 1.96$ TeV. A previous analysis [7] extracted P_u and P_d from the A_{FB} distributions measured by the D0 collaboration using 5 fb^{-1} of data in only the dielectron final state [8] and after unfolding the measured mass dependence of A_{FB} to the parton level. It demonstrated the feasibility of such a measurement and showed a tendency for P_d to be higher and P_u to be lower than expected [7]. In this paper a larger data sample and both dielectron and dimuon final states are used, thus improving the statistical precision relative to Ref. [7]. The dilepton mass distributions are not unfolded, thus removing a significant source of systematic uncertainty. As explained below, P_u and P_d in $p\bar{p}$ collisions are dominated by the valence u and d quark contributions, and their ratio, $R = P_u/P_d$, directly reflects the relative contributions of the two leading quarks inside a proton. P_u, P_d and R can also be measured using the data collected at the LHC, but measurements in pp collisions also involve sea quark contributions comparable to those of the valence quarks. The measurement presented in this paper is thus unique and provides novel

*with visitors from [a]Augustana University, Sioux Falls, SD 57197, USA, [b]The University of Liverpool, Liverpool L69 3BX, UK, [c]Deutshes Elektronen-Synchrotron (DESY), Notkestrasse 85, Germany, [d]CONACyT, M-03940 Mexico City, Mexico, [e]SLAC, Menlo Park, CA 94025, USA, [f]University College London, London WC1E 6BT, UK, [g]Centro de Investigacion en Computacion - IPN, CP 07738 Mexico City, Mexico, [h]Universidade Estadual Paulista, São Paulo, SP 01140, Brazil, [i]Karlsruher Institut für Technologie (KIT) - Steinbuch Centre for Computing (SCC), D-76128 Karlsruhe, Germany, [j]Office of Science, U.S. Department of Energy, Washington, D.C. 20585, USA, [m]University of Maryland, College Park, MD 20742, USA, [n]European Orgnaization for Nuclear Research (CERN), CH-1211 Geneva, Switzerland, [o]Purdue University, West Lafayette, IN 47907, USA, [p]Institute of Physics, Belgrade, Belgrade, Serbia, and [q]P.N. Lebedev Physical Institute of the Russian Academy of Sciences, 119991, Moscow, Russia. ‡Deceased.

information on the valence u and d quark distributions by separating them from each other and suppressing heavy quark contributions. In addition, since the sum rules in the global analysis of the parton distribution functions (PDFs) relate the valence and sea quarks, this measurement could have implications for the PDFs of sea quarks and testing the calculations of initial state gluon radiation.

At the Tevatron A_{FB} is defined as:

$$A_{FB} = \frac{N_F - N_B}{N_F + N_B},\qquad(1)$$

where N_F and N_B are the number of forward and backward events, defined as those for which $\cos\theta > 0$ and $\cos\theta < 0$, with θ defined as the angle between the direction of the negatively charged lepton and the direction of the proton beam in the Collins-Soper frame [9]. At specific values of the dilepton rapidity Y and transverse momentum Q_T defined with respect to the beam axis, the observed A_{FB} distribution as a function of the dilepton invariant mass M can be factorized as [5]:

$$A_{FB}(M) = \frac{\sum\limits_{q=u,c}[1-2D_q(M)]\sigma_q(M)}{\sigma_{\text{total}}(M)} \cdot A^u_{FB}(M)$$
$$+\frac{\sum\limits_{q=d,s,b}[1-2D_q(M)]\sigma_q(M)}{\sigma_{\text{total}}(M)} \cdot A^d_{FB}(M)$$
$$\equiv \mathcal{C}_u(M)A^u_{FB}(M) + \mathcal{C}_d(M)A^d_{FB}(M),\qquad(2)$$

where σ_q is the subprocess cross section for a specific $q\bar{q}$ ($q = u,d,s,c,b$) initial state, σ_{total} is the total cross section $\sum_{q=u,d,s,c,b}\sigma_q$, and A^u_{FB} and A^d_{FB} are asymmetries for initial up-type states ($u\bar{u}$ and $c\bar{c}$) and down-type states ($d\bar{d}$, $s\bar{s}$ and $b\bar{b}$), respectively. Forward and backward events for the $q\bar{q}$ subprocesses are defined in the Collins-Soper frame in terms of a new angle θ' between the negatively charged lepton direction and the quark direction. A^u_{FB} and A^d_{FB} are determined by $\sin^2\theta^\ell_{\text{eff}}$ and are independent of parton densities. The dilution factor D_q is defined as the probability for the $q\bar{q}$ subprocess to have an initial state where q comes from the antiproton while $\bar{q}$ comes from the proton, for which $\cos\theta = -\cos\theta'$. The weights for the up- and down-type quarks, $\mathcal{C}_u$ and $\mathcal{C}_d$, can be averaged over a finite mass range, to further separate them into mass-averaged structure parameters (P_u and P_d) and mass-dependent structure parameters (Δ_u and Δ_d) [5]:

$$\mathcal{C}_{u,d}(M) = P_{u,d} + \Delta_{u,d}(M).\qquad(3)$$

In this Letter, we have defined P_u and P_d by averaging over the mass range of [70, 116] GeV. The structure parameters, cross sections, asymmetries, and dilution factors all depend on Y and Q_T. Note that Eq. (2) factorizes the QCD part of the observed A_{FB} into $\mathcal{C}_u$ and $\mathcal{C}_d$, and the electroweak part as A^u_{FB} and A^d_{FB}.

The dilution factors D_u and D_d are modeled by the PDFs and are small since the interactions of an antiquark in the proton and a quark in the antiproton are suppressed in the relevant x-range at the Tevatron. The dilution factors for s, c and b quarks are very close to 0.5 [10–12] and thus P_u and P_d are dominated by the valence u and d quarks at leading order. As a result, P_u and P_d at the Tevatron are approximately

$$P_u \sim u(x_1)u(x_2)/\sigma_{\text{total}}(x_1,x_2),$$
$$P_d \sim d(x_1)d(x_2)/\sigma_{\text{total}}(x_1,x_2),\qquad(4)$$

where $x_{1,2}$ is the Bjorken variable for the colliding quark and antiquark respectively, defined at leading order as $x_{1,2} = \frac{\sqrt{M^2+Q_T^2}}{\sqrt{s}}e^{\pm Y}$. The ratio $R = P_u/P_d$, in which the total cross section cancels, represents the relative contribution of u and d quarks. Due to the detector acceptance discussed below, the data in this measurement has dilepton rapidity in the interval $|Y| = [0, 2.3]$. The P_u, P_d and R measured in this paper correspond to the values of x from approximately 0.004 to 0.45. We obtain information on the x-dependence of the structure parameters by analyzing the data separately for $|Y|$ intervals of [0, 0.5], [0.5, 1.0], [1.0, 1.5], and [1.5, 2.3].

This Letter focuses on the measurement of P_u and P_d. The Δ_u and Δ_d terms can be predicted with small uncertainties for M in a narrow window around the Z boson pole [5, 6]. A^u_{FB} and A^d_{FB} can be precisely predicted and have different dependences on M. P_u and P_d can be determined by comparing Eq. (2) to the measured A_{FB} distribution. The asymmetries A^u_{FB} and A^d_{FB}, and the uncertainties on A_{FB} due to the P_q and Δ_q parameters are calculated using RESBOS [13] with CT18NNLO [10] PDFs, and are shown in Fig. 1.

The D0 detector consists of a tracking system surrounded by a solenoid magnet, calorimeters, and a muon system [14–16]. Dielectron and dimuon events are collected with lepton triggers and are required to have a lepton-antilepton pair in the offline analysis. Leptons are required to be well separated from other particles both in the tracking system and the calorimeter. Muons are measured as tracks in the tracking and muon systems with $|\eta_{\text{det}}| < 1.8$ [17], and are required to have transverse momentum $p_T > 15$ GeV. Electrons are reconstructed as clusters in the central calorimeter (CC) with $|\eta_{\text{det}}| < 1.1$, and in an end calorimeter (EC) with $1.5 < |\eta_{\text{det}}| < 3.5$. They are required to have a spatially matched track in the tracking system, so that their electric charge can be determined, and also for discriminating against photons. The EC-EC events, where both electrons are in an EC, are excluded due to the high level of background for such events. The threshold for the electron transverse momentum is 25 GeV. As a result, the background contributions from $Z/\gamma^* \to \tau\tau$, W+jets, diboson (WW and WZ), $\gamma\gamma$, top quarks and multi-jets are suppressed to $\mathcal{O}(1\%)$ in the mass region $70 < M < 116$ GeV used in this analysis.
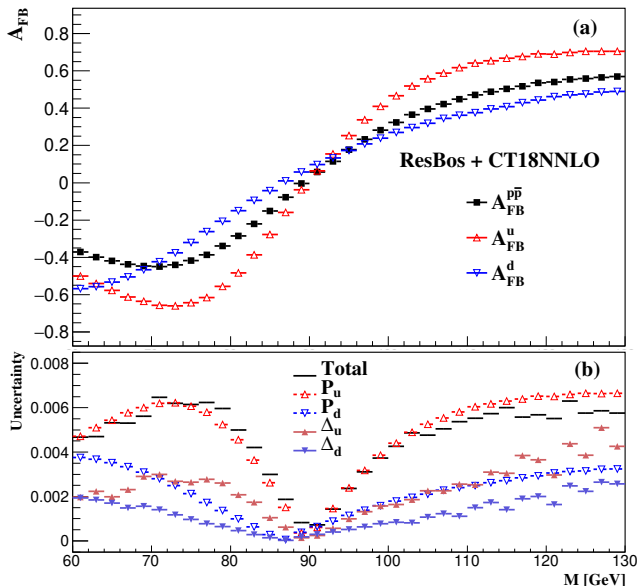
FIG. 1: (a) The PDF-independent A_{FB}^u and A_{FB}^d predicted by RESBOS as a function of M and the resulting A_{FB} in $p\bar{p}$ collisions using the CT18NNLO PDF. (b) The PDF induced absolute uncertainties in A_{FB} due to P_u, P_d, Δ_u and Δ_d.

A Monte Carlo (MC) sample of $Z/\gamma^* \to \ell^+\ell^-$ events is generated using the leading-order PYTHIA generator [18] with CT18NNLO PDFs, followed by a GEANT-based [19] simulation of the D0 detector. The samples are further corrected by reweighting the MC events at the generator level in M, Q_T, Y and $\cos\theta$ to match the calculation of RESBOS [13], which is at approximate next-to-next-to-leading order and next-to-next-to-leading logarithm in QCD. The electron energy and muon momentum are calibrated using the known resonances in the dilepton mass spectrum. The efficiencies of the online and offline selection criteria are determined using the tag-and-probe method [20] and the MC simulation is corrected to be consistent with the data. The multi-jets background is estimated using data, while other backgrounds are determined using PYTHIA MC simulations. The methodologies used to derive the energy and momentum calibrations, efficiencies and estimations of the background contributions were also employed in the previous measurements of the effective weak mixing angle [21, 22]. Many systematic effects are suppressed since A_{FB} is defined as a ratio.

For the measurement of P_u and P_d in the full $0 < |Y| < 2.3$ range or in a particular $|Y|$ interval, a set of MC template distributions of A_{FB} is prepared in which P_u and P_d are varied while keeping Δ_u and Δ_d fixed at their values calculated using RESBOS and CT18NNLO. A set of $\mathcal{C}_q = P_q + \Delta_q$ values is calculated for intervals in Y, M and Q_T [23]. A_{FB} templates are acquired by

reweighting the generator level differential cross sections $\sigma_q(Y, M, Q_T, \cos\theta)$ of the MC sample according to the $\mathcal{C}_q$ value. In the MC reweighting procedures, A_{FB}^u and A_{FB}^d are calculated using RESBOS, with $\sin^2\theta_{\text{eff}}^\ell$ set to the average of the results from the electron-positron colliders LEP and SLC [24]. Corresponding uncertainties on $\sin^2\theta_{\text{eff}}^\ell$ are extrapolated to the measured P_u and P_d. We do not use the hadron collider results on $\sin^2\theta_{\text{eff}}^\ell$ in order to avoid the influence from the specific PDF predictions used in their measurement, but this choice has a negligible impact on the result because the hadron collider measurements [25–28] give values of $\sin^2\theta_{\text{eff}}^\ell$ very close to the combined LEP/SLC result. Uncertainties on Δ_u and Δ_d are estimated using the error PDF sets given by CT18NNLO. Equation (2) is only strictly true when Y and Q_T dependences are fully considered. In this letter, the observed A_{FB} is averaged over Q_T and Y so that the factorization formalism of Eq. (2) becomes an approximation. This gives rise to additional uncertainties in the calculation of σ_q and higher order QCD contributions. Part of this uncertainty is already included when taking the CT18NNLO error PDF sets into account. The remainder is estimated by varying the Q_T distribution of RESBOS to match the predictions of PYTHIA.

P_u and P_d are determined by requiring the best agreement between the observed A_{FB} distributions in both the dielectron and dimuon events and their corresponding MC templates. Since P_u and P_d are simultaneously fitted, their values and corresponding uncertainties are correlated with a correlation coefficient $\rho = -0.859$. The central value of R and its uncertainty are calculated using the measured values and the total uncertainties of P_u and P_d, and their correlation.

The measured P_u, P_d and the ratio R in the full range $|Y| = [0, 2.3]$ is:

$$
\begin{aligned}
P_u &= 0.602 \pm 0.019(\text{stat.}) \pm 0.010(\text{theory}) \pm 0.006(\text{syst.}) \\
&= 0.602 \pm 0.022 \\
P_d &= 0.258 \pm 0.023(\text{stat.}) \pm 0.012(\text{theory}) \pm 0.005(\text{syst.}) \\
&= 0.258 \pm 0.026 \\
R &= 2.34 \pm 0.32.
\end{aligned}
$$

The systematic uncertainty corresponds to the quadratic sum of the uncertainties of imperfect efficiency determination, lepton calibration and background estimation. The theory uncertainty is the quadratic sum of the uncertainties due to Δ parameters, QCD calculation and fixed value of $\sin^2\theta_{\text{eff}}^\ell$. The systematic and theoretical uncertainties are small compared with the statistical uncertainties. Compared with the predictions of CT18NNLO, MSHT20 [11] and NNPDF4.0 [12] shown in Table I, the measured P_u is lower than the PDF predictions, while P_d is higher. This tendency is consistent with the previous measurement using 5 fb^{-1} of D0 data [7], where the mass distribution was unfolded. In the current analysis, the P_u and P_d parameters are measured by comparing the data and the simulated MC, and hence there is

no unfolding-related uncertainties. The ratio R is lower than the predictions by about 2 standard deviations (the largest difference, 2.8 standard deviations, is observed with respect to NNPDF4.0).

	P_u	P_d	R
Measured	0.602±0.022	0.258±0.026	2.34±0.32
CT18NNLO	0.636±0.011	0.213±0.009	2.99±0.16
MSHT20	0.633±0.009	0.204±0.008	3.10±0.14
NNPDF4.0	0.624±0.008	0.190±0.007	3.29±0.13

TABLE I: Measured values of P_u, P_d and R in the full $|Y|$ range $[0, 2.3]$, together with their predictions from the CT18NNLO, MSHT20 and NNPDF4.0 PDFs. Predictions are calculated using RESBOS based on the definition in Eq. (2) and Eq. (3). The measured values are presented with their total uncertainties. The theoretical predictions are calculated in the same $|Y|$ range and shown with their PDF uncertainties.

The $|Y|$-dependent measurements using both the dielectron and dimuon A_{FB} distributions are shown in Table II. The correlation coefficients of P_u and P_d in the four $|Y|$ intervals are -0.855, -0.862, -0.866 and -0.871 respectively. The comparison between the measured values and the predictions from representative PDFs is shown in Fig. 2. For $1 < |Y| < 1.5$ corresponding to $x \sim 0.2$, which is around the peak of the parton density distributions of the u and d quarks, the measured R differs from the PDF predictions by more than 3.5 standard deviations, indicating that the d quark contribution is higher than the PDF expectations. For the other three bins, the measurements of P_u and P_d show good agreement with the predictions.

$|Y|$ range	P_u	δP_u
[0, 0.5]	$0.515 \pm 0.031 \pm 0.011 \pm 0.009 \pm 0.004 \pm 0.005$	0.034
[0.5, 1.0]	$0.589 \pm 0.035 \pm 0.010 \pm 0.008 \pm 0.004 \pm 0.005$	0.038
[1.0, 1.5]	$0.568 \pm 0.036 \pm 0.007 \pm 0.010 \pm 0.005 \pm 0.003$	0.038
[1.5, 2.3]	$0.680 \pm 0.060 \pm 0.009 \pm 0.020 \pm 0.005 \pm 0.003$	0.064

$|Y|$ range	P_d	δP_d
[0, 0.5]	$0.232 \pm 0.036 \pm 0.007 \pm 0.007 \pm 0.008 \pm 0.001$	0.038
[0.5, 1.0]	$0.189 \pm 0.042 \pm 0.008 \pm 0.007 \pm 0.008 \pm 0.004$	0.044
[1.0, 1.5]	$0.348 \pm 0.046 \pm 0.005 \pm 0.008 \pm 0.010 \pm 0.002$	0.048
[1.5, 2.3]	$0.252 \pm 0.076 \pm 0.014 \pm 0.020 \pm 0.009 \pm 0.002$	0.081

$|Y|$ range	R	δR
[0, 0.5]	2.22	0.50
[0.5, 1.0]	3.11	0.90
[1.0, 1.5]	1.63	0.33
[1.5, 2.3]	2.70	1.09

TABLE II: Measurements of P_u, P_d and R in different $|Y|$ bins. The uncertainties, in order, are statistical, experimental systematic, Δ-induced, $\sin^2 \theta_{\text{eff}}^{\ell}$ and QCD modelling. The final column is the total uncertainty.

The measurements of P_u and P_d for dielectron and dimuon channels separately are given in Table III. Due to the limited detector acceptance and efficiencies for the muons, the dimuon events contribute appreciably only to the two lower $|Y|$ intervals. For both the P_u and P_d pa-
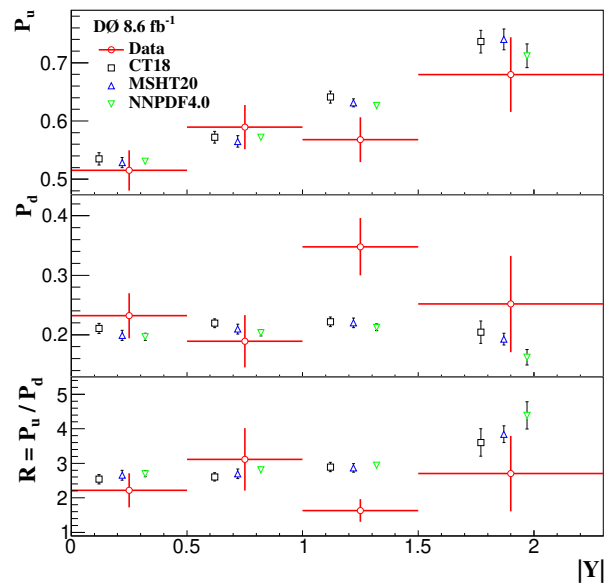

FIG. 2: Measured values of P_u, P_d and R parameters compared with the predictions of CT18NNLO, MSHT20 and NNPDF4.0. Error bars of the data points correspond to the total uncertainty of the measurement, while error bars on the predictions correspond to the PDF uncertainties. The PDF predictions are offset from the centers of the intervals for clarity.

rameters in the two lower $|Y|$ bins, the electron and muon measurements agree within 1.7 standard deviations.

$|Y|$ range		P_u	δP_u
	ee	$0.554 \pm 0.048 \pm 0.008 \pm 0.010$	0.049
[0, 0.5]	$\mu\mu$	$0.504 \pm 0.041 \pm 0.017 \pm 0.014$	0.047
	CT18NNLO	0.535 ± 0.010	
	ee	$0.528 \pm 0.049 \pm 0.010 \pm 0.010$	0.051
[0.5, 1]	$\mu\mu$	$0.656 \pm 0.054 \pm 0.017 \pm 0.013$	0.058
	CT18NNLO	0.572 ± 0.010	

$|Y|$ range		P_d	δP_d
	ee	$0.143 \pm 0.063 \pm 0.004 \pm 0.010$	0.064
[0, 0.5]	$\mu\mu$	$0.266 \pm 0.044 \pm 0.012 \pm 0.012$	0.047
	CT18NNLO	0.211 ± 0.008	
	ee	$0.270 \pm 0.066 \pm 0.007 \pm 0.011$	0.067
[0.5, 1]	$\mu\mu$	$0.124 \pm 0.055 \pm 0.013 \pm 0.012$	0.058
	CT18NNLO	0.220 ± 0.007	

TABLE III: Central values and uncertainties of the $|Y|$-dependent P_u and P_d parameters using dielectron events and dimuon events. The uncertainties, in order, are statistical, experimental systematics and theoretical systematics including PDF, $\sin^2 \theta_{\text{eff}}^{\ell}$ and QCD modelling. The last column δP_q gives the total uncertainty. Predictions of CT18NNLO are shown with corresponding PDF uncertainties.

In conclusion, we have performed a new measurement of the proton structure parameters P_u and P_d using the forward-backward asymmetry in $p\bar{p} \rightarrow Z/\gamma^* \rightarrow \ell^+\ell^-$ events using Tevatron data corresponding to 8.6 fb^{-1} of integrated luminosity. Taking advantage of the asymmetry of the weak interaction, the u and d quark contri-

butions are determined separately. For $p\bar{p}$ collisions at $\sqrt{s} = 1.96$ TeV, P_u and P_d are dominated by the valence u and d quarks for $0.004 < x < 0.45$. P_u, P_d and their ratio R are measured both for the dilepton rapidity interval $|Y| = [0, 2.3]$, and for finer $|Y|$ intervals to investigate their dependence on x. For the interval $1 < |Y| < 1.5$, the ratio of P_u and P_d differs from CT18NNLO, MSHT20 and NNPDF4.0 PDF predictions by more than 3.5 standard deviations. For the other three intervals, the results show good agreement with the PDF predictions.

[1] A. Bodek, J.-Y. Han, A. Khukhunaishvili, and W. Sakumoto, Using Drell-Yan forward-backward asymmetry to reduce PDF uncertainties in the measurement of electroweak parameters, Eur. Phys. J. C **76**, 115 (2016).

[2] E. Accomando, J. Fiaschi, F. Hautmann, and S. Moretti, Neutral current forward-backward asymmetry: from $\sin^2 \theta_W$ to PDF determinations, Eur. Phys. J. C **78**, 663 (2018).

[3] E. Accomando, J. Fiaschi, F. Hautmann, and S. Moretti, Constraining parton distribution functions from neutral current Drell-Yan measurements, Phys. Rev. D **98**, 013003 (2018), and Erratum: Phys. Rev. D **99**, 079902 (2019).

[4] Fu Yao, Siqi Yang, Minghui Liu, Liang Han, Tie-Jiun Hou, Carl Schmidt, Chen Wang and C.-P. Yuan, Reduction of PDF uncertainty in the measurement of the weak mixing angle at the ATLAS experiment, Chin. Phys. C **45**, 053001 (2021).

[5] Siqi Yang, Yao Fu, Minghui Liu, Liang Han, Tie-Jiun Hou and C.-P. Yuan, Factorization of the forward-backward asymmetry and measurements of the weak mixing angle and proton structure at hadron colliders, Phys. Rev. D **106**, 033001 (2022).

[6] Siqi Yang, Yao Fu, Minghui Liu, Renyou Zhang, Tie-Jiun Hou, Chen Wang, Hang Yin, Liang Han and C.-P. Yuan, Reduction of the electroweak correlation in the PDF updating by using the forward-backward asymmetry of Drell-Yan process, Eur. Phys. J. C, **82** 368 (2022).

[7] Mingzhe Xie, Siqi Yang, Yao Fu, Minghui Liu, Liang Han, Tie-Juin Hou, Sayipjamal Dulat and C.-P. Yuan, Measurement of the proton structure parameters in the forward-backward charge asymmetry, Phys. Rev. D **107** 054008 (2023).

[8] V. M. Abazov *et al.* (D0 Collaboration), Measurement of $\sin^2 \theta_{\text{eff}}^{\ell}$ and Z-light quark couplings using the forward-backward charge asymmetry in $p\bar{p} \rightarrow Z/\gamma^* \rightarrow e^+e^-$ events with $\mathcal{L} = 5.0$ fb^{-1} at $\sqrt{s} = 1.96$ TeV, Phys. Rev. D **84**, 012007 (2011).

[9] J. C. Collins and D. E. Soper, Angular distribution of dileptons in high-energy hadron collisions, Phys. Rev. D **16**, 2219 (1977).

[10] Tie-Jiun Hou, Jun Gao, T. J. Hobbs *et al.*, New CTEQ global analysis of quantum chromodynamics with high precision data from the LHC, Phys. Rev. D **103**, 014013 (2021).

[11] S. Bailey, T. Cridge, L. A. Harland-Lang, A. D. Martin, and R. S. Thorne, Parton distributions from LHC, HERA, Tevatron and fixed target data: MSHT20 PDFs, Eur. Phys. J. C **81**, 341 (2021).

[12] R. D. Ball et al. (NNPDF Collaboration), The path to proton structure at 1% accuracy, Eur. Phys. J. C **82**, 428 (2022).

[13] C. Balazs and C. P. Yuan, Soft gluon effects on lepton pairs at hadron colliders, Phys. Rev. D **56**, 5558 (1997).

[14] V. M. Abazov *et al.* (D0 Collaboration), The upgraded D0 detector, Nucl. Instrum. Methods Phys. Res., Sect. A **565**, 463 (2006).

[15] V. M. Abazov *et al.* (D0 Collaboration), Design and implementation of the new D0 level-1 calorimeter trigger, Nucl. Instrum. Methods Phys. Res., Sect. A **584**, 75 (2008).

[16] V. M. Abazov *et al.* (D0 Collaboration), The layer-0 inner silicon detector of the D0 experiment, Nucl. Instrum. Methods Phys. Res., Sect. A **622**, 298 (2010).

[17] We use a cylindrical coordinate system with the z axis along the proton beam direction. Pseudo-rapidity is defined as $\eta = -\ln[\tan(\theta_{\text{pol}}/2)]$ where the polar angle θ_{pol} is measured with respect to the interaction vertex. In the massless limit, η is equivalent to the rapidity

$y = (1/2) \ln[(E + p_z)/(E - p_z)]$, and η_{det} is the pseudo-rapidity measured with respect to the center of the detector.

[18] T. Sjöstrand, P. Edén, C. Feriberg, L. Lönnblad, G. Miu, S. Mrenna, and E. Norrbin, High-Energy-Physics Event Generation with PYTHIA 6.1, Comp. Phys. Commun. **135**, 238 (2001). PYTHIA version v6.323 is used throughout.

[19] R. Brun and F. Carminati, GEANT detector description and simulation tool, CERN Program Library Long Writeup W5013, 1993 (unpublished).

[20] V. M. Abazov *et al.*, (D0 Collaboration), Measurement of the shape of the boson rapidity distribution for $p\bar{p} \to Z/\gamma^* \to e^+e^- + X$ events produced at $\sqrt{s} = 1.96$ TeV, Phys. Rev. D **76**, 012003 (2007).

[21] V. M. Abazov *et al.* (D0 Collaboration), Measurement of the Effective Weak Mixing Angle in $p\bar{p} \to Z/\gamma^* \to e^+e^-$ Events, Phys. Rev. Lett. **115**, 041801 (2015).

[22] V. M. Abazov *et al.* (D0 Collaboration), Measurement of the Effective Weak Mixing Angle in $p\bar{p} \to Z/\gamma^* \to \ell^+\ell^-$ Events, Phys. Rev. Lett. **120**, 241802 (2018).

[23] We use a bin size of 1 GeV for the M-dependence and a bin size of 0.1 for the Y-dependence. For the Q_T-dependence, the bin size is 1 GeV, 10 GeV and 100 GeV for $Q_T < 10$, $10 < Q_T < 50$ and $50 < Q_T < 250$ GeV respectively.

[24] G. Abbiendi *et al.* (LEP Collaborations ALEPH, DELPHI, L3 and OPAL, SLD Collaboration, LEP Electroweak Working Group, SLD Electroweak and Heavy Flavor Groups), Precision electroweak measurements on the Z resonance, Phys. Rep. **427**, 257 (2006).

[25] T. Aaltonen *et al.* (CDF and D0 Collaborations), Tevatron Run II combination of the effective leptonic electroweak mixing angle, Phys. Rev. D **97**, 112007 (2018).

[26] ATLAS public note at https://atlas.web.cern.ch/Atlas/GROUPS/PHYSICS/CONFNOTES/ATLAS-CONF-2018- 037/(2018).

[27] A. M. Sirunyan *et al.* (CMS Collaboration), Measurement of the weak mixing angle using the forward-backward asymmetry of Drell-Yan events in pp collisions at 8 TeV, Eur. Phys. J. C **78**, 701 (2018).

[28] R. Aaij *et al.* (LHCb Collaboration), Measurement of the forward-backward asymmetry in $Z/\gamma^* \to \mu^+\mu^-$ decays and determination of the effective weak mixing angle, JHEP **11**, 190 (2015).